Title

Control of a neuronal morphology program by an RNA-binding zinc finger protein, Unkempt

Journal

Genes & Development, 29(5)

ISSN

0890-9369

Authors

Murn, Jernej
Zarnack, Kathi
Yang, Yawei J
et al.

Publication Date

2015-03-01

DOI

10.1101/gad.258483.115

Peer reviewed

Control of a neuronal morphology program by an RNA-binding zinc finger protein, Unkempt

Jernej Murn,[1,2] Kathi Zarnack,[3,4] Yawei J. Yang,[5,6,7,8,9,10] Omer Durak,[11,12] Elisabeth A. Murphy,[5,6,7,8,9,10] Sihem Cheloufi,[13,14] Dilenny M. Gonzalez,[5,6,7,8,9,10] Marianna Teplova,[15] Tomaž Curk,[16] Johannes Zuber,[17] Dinshaw J. Patel,[15] Jernej Ule,[18] Nicholas M. Luscombe,[3,19,20,21] Li-Huei Tsai,[11,12] Christopher A. Walsh,[5,6,7,8,9,10] and Yang Shi[1,2]

[1]Department of Cell Biology, Harvard Medical School, Boston, Massachusetts 02115, USA; [2]Division of Newborn Medicine, Boston Children's Hospital, Boston, Massachusetts 02115, USA; [3]European Molecular Biology Laboratory (EMBL) European Bioinformatics Institute, Hinxton, Cambridge CB10 1SD, United Kingdom; [4]Buchmann Institute for Molecular Life Sciences, Goethe University Frankfurt, 60438 Frankfurt am Main, Germany; [5]Division of Genetics and Genomics, [6]Manton Center for Orphan Disease Research, Boston Children's Hospital, Boston, Massachusetts 02115, USA; [7]Department of Pediatrics, [8]Department of Neurology, Harvard Medical School, Boston, Massachusetts 02115, USA; [9]Broad Institute of Massachusetts Institute of Technology and Harvard, Cambridge, Massachusetts 02142, USA; [10]Howard Hughes Medical Institute, Chevy Chase, Maryland 20815, USA; [11]Picower Institute for Learning and Memory, [12]Department of Brain and Cognitive Sciences, Massachusetts Institute of Technology, Cambridge, Massachusetts 02139, USA; [13]Cancer Center, [14]Center for Regenerative Medicine, Massachusetts General Hospital, Boston, Massachusetts 02114, USA; [15]Structural Biology Program, Memorial Sloan-Kettering Cancer Center, New York, New York 10065, USA; [16]Faculty of Computer and Information Science, University of Ljubljana, 1000 Ljubljana, Slovenia; [17]The Research Institute of Molecular Pathology, Vienna Biocenter, 1030 Vienna, Austria; [18]Department of Molecular Neuroscience, University College London Institute of Neurology, London WC1N 3BG, United Kingdom; [19]UCL Genetics Institute, Department of Genetics, Environment, and Evolution, University College London, London WC1E 6BT, United Kingdom; [20]Cancer Research UK London Research Institute, London WC2A 3LY, United Kingdom; [21]Okinawa Institute for Science and Technology Graduate University, Onna-son, Kunigami-gun, Okinawa 904-0495, Japan

Cellular morphology is an essential determinant of cellular function in all kingdoms of life, yet little is known about how cell shape is controlled. Here we describe a molecular program that controls the early morphology of neurons through a metazoan-specific zinc finger protein, Unkempt. Depletion of Unkempt in mouse embryos disrupts the shape of migrating neurons, while ectopic expression confers neuronal-like morphology to cells of different nonneuronal lineages. We found that Unkempt is a sequence-specific RNA-binding protein and identified its precise binding sites within coding regions of mRNAs linked to protein metabolism and trafficking. RNA binding is required for Unkempt-induced remodeling of cellular shape and is directly coupled to a reduced production of the encoded proteins. These findings link post-transcriptional regulation of gene expression with cellular shape and have general implications for the development and disease of multicellular organisms.

[*Keywords*: RNA-binding proteins; cell morphology; gene expression program; neurons; translation; Unkempt]

Supplemental material is available for this article.

Received January 9, 2015; revised version accepted February 6, 2015.

Cellular shape is one of the most distinctive features of somatic cells in multicellular organisms and is intimately linked with cellular function. Numerous descriptions of in vitro cell fate conversion experiments (Davis et al. 1987; Vierbuchen et al. 2010; Sato et al. 2011) as well as spontaneous morphogenesis of dissociated primary cells in culture (Dotti et al. 1988) suggest that the basic instructions for morphology of a particular cell type are intrinsically encoded; i.e., specified at the time of cell lineage commitment. However, it is largely unknown how cell shape is determined and to what extent it is programmed.

The emergence and homeostasis of complex cellular phenotypes, including cell shape, are critically dependent

Corresponding authors: yang_shi@hms.harvard.edu, murn.jernej@gmail.com
Article is online at http://www.genesdev.org/cgi/doi/10.1101/gad.258483.115.

on specific gene regulatory programs (Niehrs and Pollet 1999). Spatiotemporal organization of gene expression, which is of particular relevance to cellular morphology, relies heavily on the control of post-transcriptional events, including mRNA export, stability, and translation, to sustain cellular homeostasis. RNA-binding proteins (RBPs) can synchronize the fates of multiple RNA molecules by binding to particular secondary structures or sequences present in some RNAs but not others (Keene 2007; Li et al. 2010; Ray et al. 2013). Moreover, genome-wide studies have found that by selective targeting, individual RBPs coordinate post-transcriptional processing of whole cohorts of functionally related RNAs. Such functionally coherent protein–RNA units, also known as "RNA operons" (Keene 2007), substantially expand the regulatory plasticity of the genomes, endowing cells with tissue-specific functions and allowing for swift cellular responses to the changing microenvironment.

A group of CCCH-type zinc finger proteins has been associated with different aspects of cellular asymmetry, and several family members have shown the capacity to rapidly alter gene expression programs. Contrary to the general notion that zinc finger domains bind DNA, the CCCH motif is thought to specialize in the recognition of RNA (Hall 2005; Lunde et al. 2007; Liang et al. 2008). Accordingly, the majority of the studied CCCH family members regulate different post-transcriptional processes across species, and several have been associated with human disease, including myotonic dystrophy (Miller et al. 2000; Wang et al. 2012), autoimmune disorders (Vinuesa et al. 2005; Uehata et al. 2013), and cancer (Rounbehler et al. 2012). However, despite their coordinated control of physiologically related genes and their relevance to human disease, the roles of most of the CCCH zinc finger proteins are still poorly understood.

Unkempt is a conserved family member that harbors a set of six tandem CCCH motifs, the largest such array in the human genome (Fig. 1A; Liang et al. 2008). Initially described in 1992 as an embryonically expressed gene in fruit flies, *unkempt* was shown to be essential for early development; its homozygous deletion led to larval lethality, while heterozygous flies carrying a hypomorphic allele displayed an "unkempt" phenotype (Mohler et al. 1992). Another recent report identified Unkempt as a neurogenic component of the mTOR pathway, suggesting that it may act as a negative regulator of photoreceptor differentiation in fruit flies (Avet-Rochex et al. 2014). However, the exact function of Unkempt has remained obscure. We hypothesized that Unkempt might regulate a gene expression program with a critical role for a distinct aspect of cellular physiology or development of specific cell lineages.

Results

Unkempt is conserved across metazoans and is enriched in embryonic brains

Taking evolutionary conservation as a measure of functional significance, we looked for bona fide orthologs of human Unkempt protein and found them across the animal kingdom but not in plants or fungi (Fig. 1B;

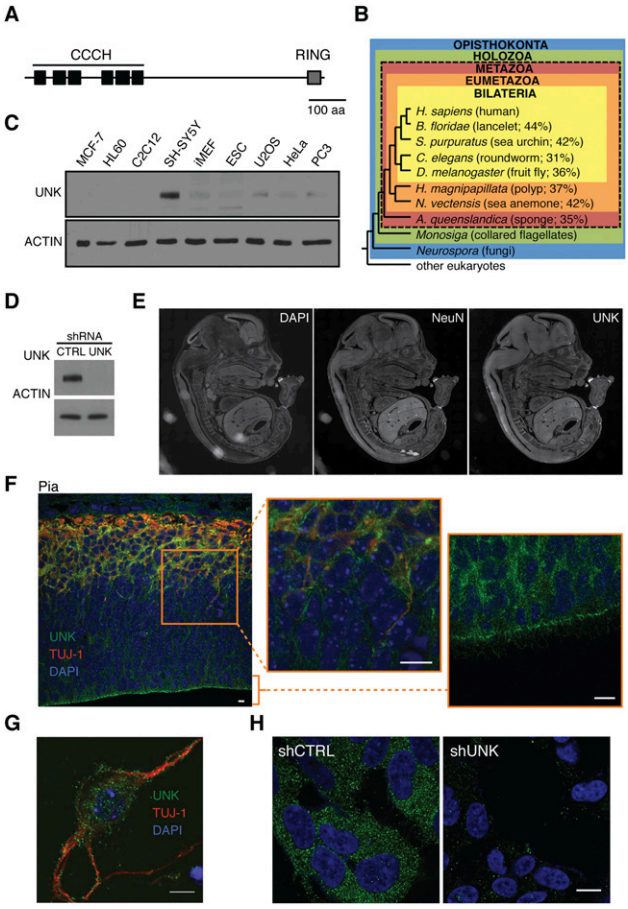

Figure 1. Evolutionary conservation and expression of Unkempt. (*A*) Sketch of the human Unkempt protein showing the relative positions of the six tandem CCCH zinc finger motifs and a RING finger domain. Bar, 100 amino acids. (*B*) Unkempt protein is conserved across metazoans. The cladogram shows the percentage of amino acid identities of Unkempt orthologs found in each of the indicated species compared with the full-length human ortholog. Note that no orthologs of Unkempt are found in nonmetazoan species. Evolutionary relationships of animals shown are based on Srivastava et al. (2010). (Adapted by permission from Macmillan Publishers Ltd., © 2010.) RefSeq protein accession numbers of all of the indicated Unkempt orthologs are listed in Supplemental Figure S1A. (*C*) Detection of Unkempt (UNK) in continuous cell lines by immunoblotting. (*D*,*H*) Depletion of endogenous Unkempt in SH-SY5Y cells detected by immunoblotting (*D*) and immunofluorescence (*H*) using Unkempt-specific antibodies. Bar, 10 μm. (*E*) Immunohistochemistry of mouse E15 whole embryo sagittal sections revealing highly enriched expression of Unkempt in the CNS. The location of the CNS is highlighted by the expression of the neuronal marker NeuN. See also Supplemental Figure S1D. (*F*) Expression of Unkempt in the cortex of E15 mouse embryos. The cortical wall was probed with antibodies against Unkempt (green) and neuronal marker Tuj-1 (red) and counterstained with DAPI to label the nuclei (blue). The highlighted region (orange rectangle) is shown magnified (*middle*), along with a close-up of the ventricular zone (*right*), together indicating a pervasive expression of Unkempt throughout the cortical wall. Bars, 10 μm. (*G*) Immunocytochemistry of dissociated E15 neurons in vitro showing the expression of Unkempt and the neuronal marker Tuj-1. Bar, 10 μm.

Supplemental Fig. S1A). Multiple sequence alignment analysis revealed a particularly deep evolutionary conservation of all six tandemly arrayed CCCH zinc fingers (Supplemental Fig. S1B). A query of the published expression profiles of a wide range of mouse tissues and cell lines found most abundant transcripts of *Unkempt* in mouse neuroblastoma cells, consistent with its mRNA locating to the CNS of a fly larva (Supplemental Fig. S1C; Mohler et al. 1992). This observation was confirmed in our survey of continuous cell lines and whole mouse embryos that revealed the highest expression of Unkempt protein in a human cell line of neuronal origin (SH-SY5Y) and CNS, respectively (Fig. 1C–E; Supplemental Fig. S1D). Unkempt appeared particularly abundant in mature neurons, where it partitioned into mainly cytoplasmic puncta, similar to the pattern seen in SH-SY5Y cells (Fig. 1F–H; Supplemental Fig. S1E,F). Whole mouse brains at different stages of development showed induction of Unkempt at embryonic day 12 (E12) and a decline postnatally (Supplemental Fig. S1G). The rough temporal overlap with the peak of neurogenesis and structuring of the brain suggested a broad regulatory role of Unkempt during the formation of the CNS.

Control of early neuronal morphology and reshaping of nonneuronal cells by Unkempt

To examine the function of Unkempt in vivo, we carried out in utero electroporation of plasmids expressing shRNA and a fluorescent reporter to acutely silence Unkempt in the developing CNS of mouse embryos. Immunostaining of electroporated cortexes revealed a significant impact on neuronal migration, and this effect persisted postnatally (Fig. 2A,B; Supplemental Fig. S2A–C). The observed defect in neuronal migration could be rescued by coexpression of RNAi-resistant wild-type Unkempt but not mutant Unkempt proteins lacking portions of the CCCH zinc finger domain (Fig. 2A,B; see below). Upon a closer inspection of cellular morphology as a key parameter in neuronal migration, we noticed that

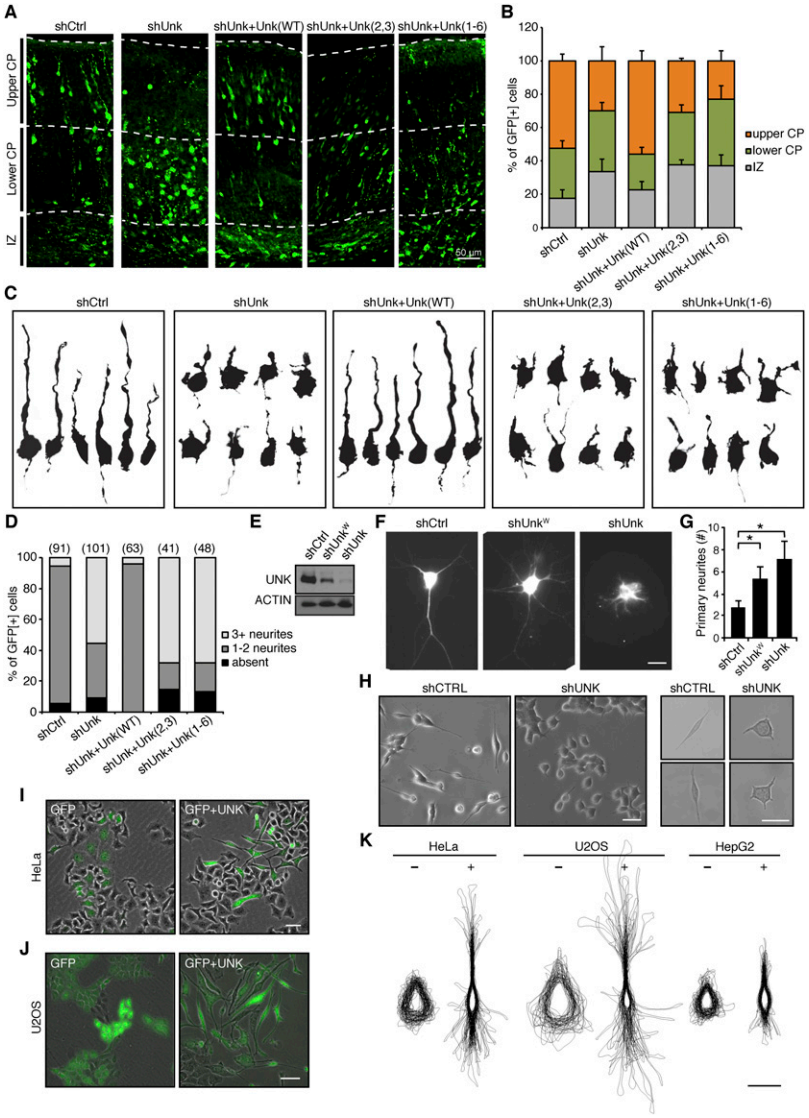

Figure 2. Unkempt is required for the early neuronal morphology and is sufficient to polarize cells of nonneuronal origin. (*A*,*B*) Impaired migration of Unkempt-deficient neurons. (*A*) Cortical sections of mouse embryos electroporated at E14.5 with the indicated constructs and analyzed at E19. Electroporated neurons are in green. Unk(WT), Unk(2,3), and Unk(1–6) are RNAi-resistant wild-type Unkempt, mutant missing zinc fingers 2 and 3, and mutant missing zinc fingers 1–6 (see also Fig. 3A). (IZ) Intermediate zone; (CP) cortical plate. (*B*) Quantification of electroporated neurons as shown in *A*. The data are based on the evaluation of at least 1000 cells per condition. (*C*,*D*) Morphological analysis of migrating neurons. (*C*) Computationally reconstructed shapes of GFP-positive neurons from the lower cortical plate of E19 embryos electroporated with the indicated constructs. (*D*) Quantification of GFP-positive neurons as in *C* by the number of primary neurites per cell. The number of cells quantified for each indicated condition is shown in parentheses *above* each column. (*E*) Efficiency of the RNAi constructs used in explanted neurons in vitro. (*F*,*G*) Impaired morphogenesis of Unkempt-depleted cortical neurons in vitro (*F*) with quantification of primary neurites per cell (*G*). (*) $P < 0.001$, Student's *t*-test. Bar, 10 μm. (*H*) Representative images of SH-SY5Y cells growing in clusters (*left*) or individually (*right*). Bars, 50 μm. (*I*,*J*) GFP-inducible or GFP and Unkempt-inducible HeLa cells at 36 h (*I*) and U2OS cells at 72 h (*J*) of treatment with Dox. Bars, 50 μm. (*K*) Overlaid outlines of GFP-inducible (–) or GFP and Unkempt-inducible (+) HeLa, U2OS, and HepG2 cells at 72 h of treatment with Dox. Error bars represent SD. Bar, 25 μm.

the majority of the poorly migrating, Unkempt-deficient neurons had abnormally round cell bodies and extended short and numerous neurites (Fig. 2C,D; Supplemental Fig. S2D). This was in contrast to the control as well as knockdown neurons rescued with RNAi-resistant wild-type Unkempt, both of which displayed a typical bipolar shape that normally allows the migrating neurons to reach their final positions in the brain (Fig. 2C,D; Noctor et al. 2004). These data suggest that Unkempt is mandatory for the early morphology of neurons during embryonic development of mice.

As the shape of neurons is influenced by a variety of intracellular and extracellular cues, we next asked whether Unkempt regulates neuronal morphology in a cell-autonomous manner. To that end, we ablated the expression of Unkempt in explanted cortical neurons and followed their morphogenesis in vitro. Similar to the phenotype observed in utero, knockdown of Unkempt in isolated neurons led to a reduction in neurite length and a dose-dependent increase in the number of primary neurites compared with control (Fig. 2E–G). Moreover, silencing of Unkempt in human SH-SY5Y cells converted the early neuronal-like cellular shape into a rounder morphology with shorter but more numerous processes, akin to the change seen in vivo (Fig. 2H). Together, these results indicate a cell-autonomous role of Unkempt in the establishment and maintenance of the early morphology of cortical neurons.

The broad expression pattern suggested that Unkempt might be required for shaping other types of neurons in the CNS as well. We thus wished to explore the possibility that the morphogenetic effect of Unkempt might be cell type-independent and limited solely by its expression. We selected a set of continuous cell lines of diverse but nonneuronal origin, including HeLa, U2OS, HepG2, and immortalized mouse embryonic fibroblasts (iMEFs), and engineered them to inducibly express a reporter-traceable exogenous Unkempt upon doxycycline (Dox) treatment (Supplemental Fig. S2E). Remarkably, as early as 12 h after the addition of Dox, the inducible cells began to show morphological changes, and some adopted a spindle-like shape (Supplemental Fig. S2F). This phenotype became progressively more evident upon longer periods of induction, with the cells displaying an overt bipolar morphology (Fig. 2I–K; Supplemental Fig. S2F–M). None of the established polarity components, including PAR complex proteins, CDC42, Smurf2, and others that we tested in this system, was able to recapitulate the Unkempt-induced phenotype, signifying the unique role of Unkempt in cell morphogenesis (Supplemental Fig. S2N, O). We observed no induction of neuronal markers, including NeuN, Tuj-1, Pax6, vimentin, or nestin, even after extended periods of treatment with Dox, arguing against transdifferentiation of cells toward neuronal fate (data not shown). The fact that ectopic Unkempt induces a similar phenotype in cells of unrelated origin suggests that Unkempt engages components of a specific morphology program that are not endemic to neurons but are expressed ubiquitously.

Unkempt-driven cell morphogenesis requires mRNA binding

Given the highest degree of sequence conservation within the CCCH zinc finger domain of Unkempt (Supplemental Fig. S1B), we hypothesized that this structural element might present a critical determinant of Unkempt-driven shaping of cells. We performed a structure–function analysis in which we deleted different segments of the inducible Unkempt protein and investigated the impact of the created mutants on cellular shape (Fig. 3A; Supplemental Fig. S2K). Unkempt lacking any portion of the zinc finger domain failed to induce a bipolar phenotype,

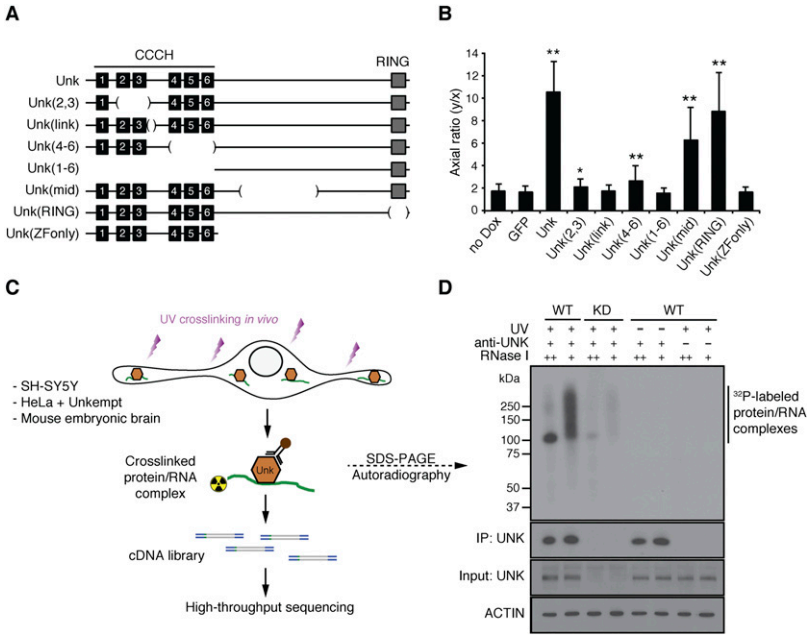

Figure 3. Structure–function analysis and identification of Unkempt as an RBP. (*A*) A series of deletion mutants of Unkempt protein examined for their capacity to impact cellular morphology. Internal deletions are indicated by bracketed regions. (*B*) The morphologies of HeLa cells inducibly expressing GFP alone or GFP and either of the indicated Unkempt mutants were quantified by calculating their axial ratios (see Supplemental Fig. S2K). The results are compared with GFP control. (*) $P = 0.0007$; (**) $P < 0.0001$. (*C*) Outline of the Unkempt iCLIP experiment coupled with deep sequencing (see also Supplemental Table S1). (*D*) Binding of Unkempt to RNA in SH-SY5Y cells. (*Top*) Autoradiogram. The *bottom* three stripes are immunoblots of UNK and Actin. (WT) Wild-type; (KD) knockdown.

whereas mutants lacking the C-terminal portions induced the bipolar morphology in a manner similar to full-length Unkempt (Fig. 3B; Supplemental Fig. S3A). These data highlight an essential role for the CCCH zinc fingers, a putative RNA-binding domain, in the Unkempt-driven morphological transformation of cells.

To investigate the RNA-binding capacity of Unkempt, we made use of iCLIP (individual nucleotide resolution UV cross-linking and immunoprecipitation), a stringent method that allows for genome-wide detection as well as precise mapping of protein–RNA interactions in living cells (Fig. 3C; Konig et al. 2010). Affinity purification of endogenous Unkempt from UV-irradiated SH-SY5Y cells followed by SDS-PAGE separation revealed the presence of a single complex that corresponded in size to Unkempt bound to labeled RNA (Fig. 3D). The signal produced by this complex was dependent on the dose of the added RNase I, diminished upon knockdown of Unkempt, and undetectable when either UV irradiation or Unkempt-specific antibodies were omitted. A similar signal was obtained with Unkempt protein overexpressed in HeLa cells or endogenous Unkempt in mouse embryonic brains (see below), demonstrating the occurrence of Unkempt–RNA interactions in vivo. Importantly, in contrast to the wild-type Unkempt, the inactive Unkempt mutants lacking either the entire zinc finger domain or a part thereof showed no appreciable affinity for RNA (Supplemental Fig. S3B). Moreover, unlike the wild-type Unkempt, RNA-binding-deficient mutant proteins were unable to rescue the aberrant neuronal migration or the morphological abnormalities of Unkempt-deficient neurons (Fig. 2A–D; Supplemental Fig. S2A–D). Taken together, these results indicate a requirement for RNA binding by Unkempt in the establishment of bipolar cell morphology in vitro and in vivo.

To identify the RNA species targeted by Unkempt, we carried out RT–PCR amplification of the UV cross-linked RNA followed by high-throughput sequencing of the prepared cDNA libraries (Supplemental Fig. S3C). We performed iCLIP experiments in three to five replicates in each of the three biological contexts in which we observed Unkempt-dependent cell morphology; namely, in SH-SY5Y cells, whole brains of E15 mouse embryos, and HeLa cells ectopically expressing Unkempt (Supplemental Table S1). Genomic annotation of cDNA sequences found up to 90% of all Unkempt-binding events mapping to mRNAs, with more than half of all binding sites mapping to coding sequences (CDSs) (Fig. 4A,B.) Importantly, we observed little correlation between the number of iCLIP tags per transcript and either transcript length or abundance, indicating a highly selective manner in which Unkempt binds its RNA targets (Supplemental Fig. S4A,B).

To determine the identities of mRNAs bound by Unkempt, we only considered iCLIP tags that mapped to regions within mature transcripts and could be unambiguously assigned to a specific gene. By taking into account a particular binding pattern of Unkempt (see below), reproducibility of binding, and the combined number of unique iCLIP tags, we identified 1186, 1020, and 649 Unkempt mRNA targets that repeatedly scored in SH-SY5Y cells, HeLa cells, and embryonic brains, respectively (Supplemental Table S2A–C). Comparison of the three data sets defined a core subset of 263 genes that were bound by Unkempt in all three sample types displaying Unkempt-dependent cellular morphology (Supplemental Fig. S4C; Supplemental Table S2D). While this list contains bona fide mRNA targets of Unkempt, it is likely incomplete due to the conservative selection criteria restricting identification of low-abundance targets.

Functional annotation of Unkempt mRNA targets strongly pointed to their involvement in general processes related to protein metabolism and trafficking (Fig. 4C; Supplemental Table S3). This was in contrast to several previously studied RBPs—including NOVA proteins, fragile X mental retardation protein (FMRP), and neuronal Elav-like proteins—that primarily regulate neural-specific, largely synapse-related, transcripts in the brain (Ule et al. 2005; Darnell et al. 2011; Ince-Dunn et al. 2012; Wagnon et al. 2012). A separate analysis of Unkempt targets interrogating canonical pathways revealed a strong enrichment of molecules implicated in translation initiation and p70S6K signaling, the protein ubiquitination pathway,

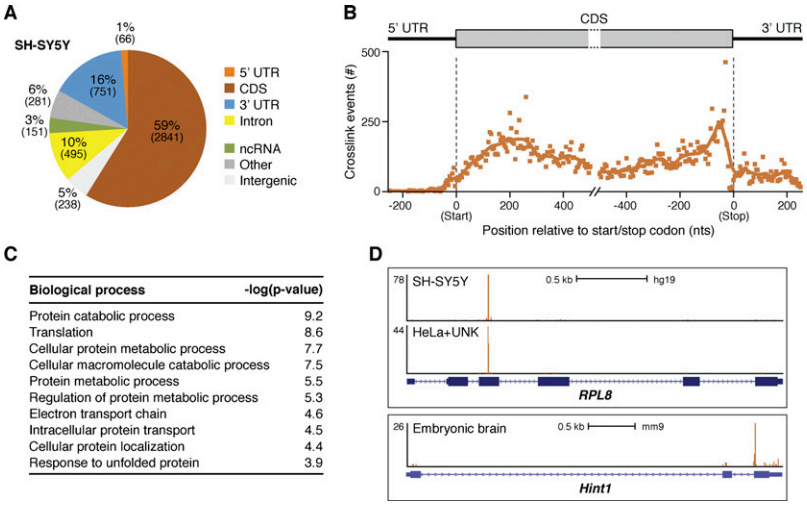

Figure 4. Unkempt-bound RNA species and the mode of RNA binding. (*A*) Distribution of Unkempt iCLIP tag clusters among different RNA segments in SH-SY5Y cells. Similar distributions of clusters were observed in HeLa cells and embryonic brains (data not shown). (*B*) Metatranscript analysis showing the positional frequency of Unkempt binding sites along the length of all target mRNAs in SH-SY5Y cells. (*C*) Gene ontology (GO) analysis of Unkempt target transcripts in SH-SY5Y cells. The top 10 GO terms are ranked by their *P*-values. (see also Supplemental Table S3). (*D*) Unkempt contacts its target transcripts commonly at just one dominant binding site. Snapshots from the University of California at Santa Cruz Genome Browser (http://genome.ucsc.edu; human assembly GRCh37/hg19 and mouse assembly GRCm38/mm10; Kent et al. 2002) of different Unkempt target genes depict binding positions in the indicated sample types (see also Supplemental Fig. S6A).

and signaling by the Rho and Ran families of GTPases (Supplemental Fig. S4D; Supplemental Table S4). Together, these analyses indicate that much of the Unkempt-bound transcriptome is represented by mRNAs functionally linked to protein turnover in addition to transcripts encoding proteins with direct roles in regulating cellular shape.

To probe the functional dependence of Unkempt-induced cellular morphology, we carried out a focused loss-of-function screen in inducible HeLa cells by silencing the expression of 34 of the strongest Unkempt targets and, as a control, an equal number of nontargeted molecules with known roles in morphology-related processes (Supplemental Fig. S5A,B; Supplemental Table S5). Although depletion of no single molecule, except Unkempt itself, completely suppressed the reshaping of cells upon induction of Unkempt, several of the tested components exhibited milder phenotypic effects. Notably, only a small proportion of the nontargeted molecules (11 of 34; 32%) affected the Unkempt-induced morphology despite their known roles in cell shape control. In contrast, knockdown of close to half (16 of 34; 47%) of the strongly bound target genes interfered with cell morphogenesis, many of them (e.g., S100A11, PSMD12, CCT5, and HSPA8) without a prior record in cell shape regulation (Supplemental Fig. S5B). Because of the particular regulatory function of Unkempt and its mode of RNA binding (see below), we further examined the effects of several of the identified molecules by perturbing their levels through overexpression of the corresponding cDNAs lacking Unkempt-binding sites (Supplemental Fig. S5C,D; see below). Notably, only those target molecules that scored in the loss-of-function screen moderately suppressed the reshaping of cells upon overexpression, suggesting that expression levels of these Unkempt target genes play a critical role in Unkempt-induced cell morphogenesis (Supplemental Fig. S5E). These results point to the complexity of the process and suggest that Unkempt acts as a hub to coordinate not one but rather a multitude of molecular pathways to bring about a morphological transformation of cells.

A unique mode of RNA binding and the Unkempt recognition element

Global analysis of all binding sites showed their ubiquitous distribution within the CDS as the most densely populated mRNA segment (Fig. 4B). However, the examination of occupancy of Unkempt on individual transcript targets revealed unique, narrowly defined sites of contact, commonly with just one dominant binding site on the message (Fig. 4D; Supplemental Fig. S6A). This pattern differs markedly from those reported for other CDS-binding RBPs (including FMRP and LIN28) that exhibit a broad distribution of binding sites along the coding regions of mRNAs (Darnell et al. 2011; Cho et al. 2012). The precise positions of Unkempt target sites were well conserved between SH-SY5Y cells and the inducible HeLa cells, indicating the maintained specificity for RNA binding regardless of whether Unkempt was expressed endogenously or forcefully introduced into cells (Fig. 4D; Supplemental Fig. S6A).

To examine the RNA sequence specificity of Unkempt, we searched for enrichment of all possible pentamers in the vicinity of the cross-link sites (Fig. 5A,B). With some variation between different sample types, two motifs emerged from all iCLIP data sets: a U-rich motif and a U/A/G-containing motif (Fig. 5B). To resolve this dichotomy, we aligned sequences spanning the cross-link sites of several strongly bound transcripts and found a U-rich region almost invariably located precisely at the cross-link sites (Fig. 5A,C). A further manual inspection identified a common UAG trimer at a distance of just a few nucleotides 5′ to the cross-link site (Fig. 5C). A global analysis of all Unkempt target transcripts confirmed a marked enrichment of the UAG motif consistently occurring just upstream of the cross-link sites in all three sample types (Fig. 5D). This fixed linear arrangement of the UAG triplet and the U-rich stretch suggested that both motifs might contribute to target recognition by Unkempt.

To evaluate the functional relevance of these results, we first performed electrophoretic mobility shift assay (EMSA) using short synthetic RNAs as substrates for a full-length, recombinant mouse Unkempt protein (Supplemental Fig. S6B). Wild-type sequences encompassing binding sites of two Unkempt target mRNAs—human *HSPA8* and mouse *Ptn*—bound to Unkempt with a dissociation constant in the nanomolar range (Fig. 5E). Markedly, mutating the UAG trimer essentially abolished any detectable affinity of RNA for Unkempt (Fig. 5E). Randomization of the nucleotides outside of either deduced motif did not affect the binding, while alterations of the UAG trimer in the context of a randomer, including single nucleotide substitutions, substantially reduced the affinity of Unkempt for RNA (Fig. 5E; Supplemental Fig. S6C). The U-rich region displayed a smaller but noticeable effect on binding; replacement of U's with A's preserved the affinity, while substitutions with C's or G's resulted in decreased binding. Together, these data identify a consensus Unkempt recognition element consisting of a mandatory UAG trimer upstream of a U/A-rich motif. Globally, we found this element present within binding sites of 56%–72% of mRNAs targets, indicating its dominant role as a specificity determinant for binding by Unkempt (Supplemental Fig. S6D; Supplemental Table S2). The cross-link sites of Unkempt thus appear shifted to only one of the two binding motifs within the Unkempt-binding element, likely due to a slight uridine bias of the UV light (Sugimoto et al. 2012).

We further examined the RNA-binding affinity of Unkempt by using isothermal titration calorimetry (ITC) to monitor the binding of the zinc finger domain encompassing all six CCCH zinc fingers (ZF1–6) or, separately, either of the two sets of three highly conserved zinc fingers (ZF1–3 and ZF4–6) to the *HSPA8*-binding site (Fig. 5F). While each set of three zinc fingers bound to the 18-mer RNA with a moderate affinity (K_d^{ZF1-3} = 5.0 μM, and K_d^{ZF4-6} = 1.6 μM), the entire CCCH domain bound to the same oligonucleotide with a significantly lower dissociation constant (K_d^{ZF1-6} = 0.2 μM), suggesting a cooperative binding of RNA by the zinc fingers of Unkempt.

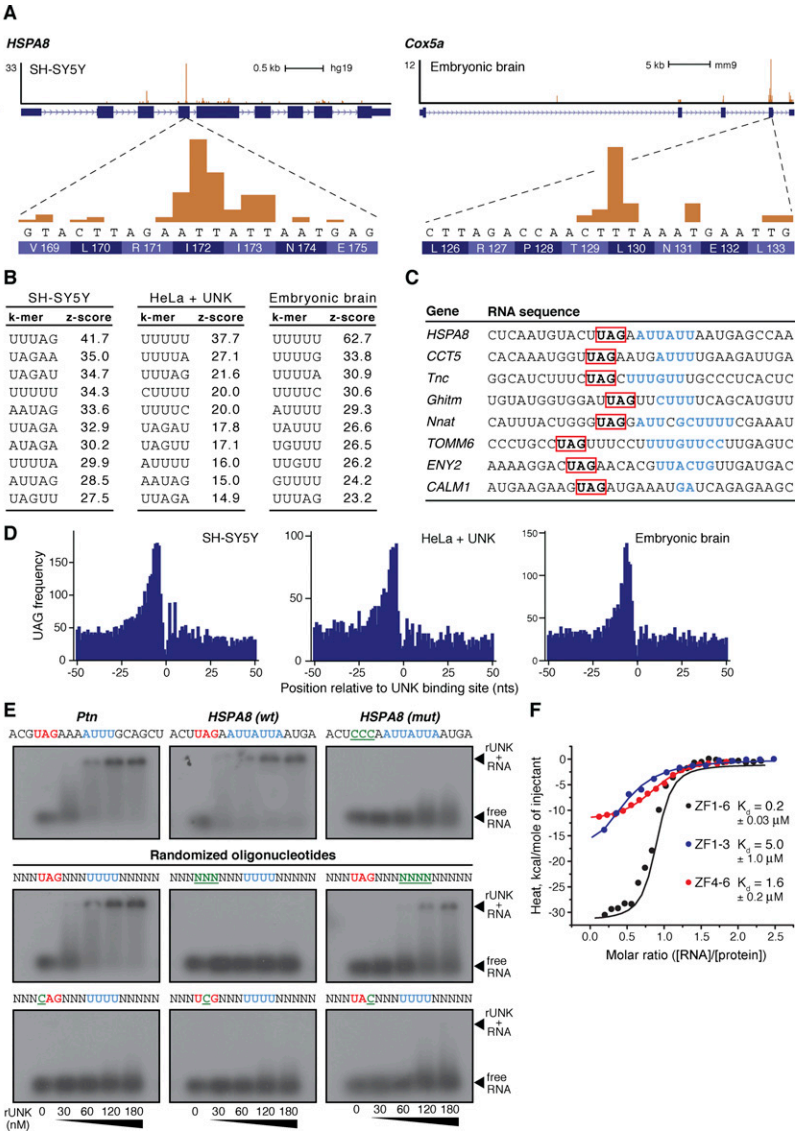

Figure 5. The RNA recognition element of Unkempt. (*A*) Magnified regions of two Unkempt target genes revealing DNA sequences and the encoded amino acids at each major cross-link site. (*B*) k-mer analysis in the vicinity of all cross-link sites for each sample type. The most highly enriched RNA pentamers are ranked by the *Z*-score. (*C*) Alignment of several target mRNA regions harboring the major cross-link sites (blue) and the identification of the conserved UAG motif (red). (*D*) Global enrichment of the UAG motif in the vicinity of Unkempt-binding sites on target mRNAs. (*E*) EMSA demonstrating a binding requirement for the intact UAG motif (red) and enhanced RNA binding of recombinant Unkempt (rUnk) in the presence of the U/A-rich motif (blue). Mutations within either binding motif are highlighted in green and underlined. Nanomolar concentrations of rUnk used in all assays are indicated (see also Supplemental Fig. S6C). (*F*) ITC binding curves of complex formation between the indicated domains of Unkempt and the 18-mer *HSPA8*-binding site. (K_d) Dissociation constant.

Unkempt reduces translational efficiency of target mRNAs

To understand the functional significance of mRNA binding by Unkempt, we first considered the possibility that Unkempt may regulate the stability of its target transcripts, analogous to some other CCCH family members (Carballo et al. 1998; Matsushita et al. 2009; Leppek et al. 2013). However, differential expression analysis upon depletion of Unkempt in SH-SY5Y cells showed little correlation with the number of iCLIP tags per transcript and suggested that, overall, the RNA binding did not have an impact on the steady-state levels of the targeted messages (Supplemental Fig. S7A,B).

The binding preference for coding regions led us to speculate that Unkempt may regulate translation of its bound messages, analogous to some other CDS-binding RBPs (Fig. 4A,B; Abdelmohsen et al. 2011; Darnell et al. 2011; Cho et al. 2012; Brummer et al. 2013). To determine whether Unkempt associates with polyribosomes, we fractionated the lysates of SH-SY5Y cells and mouse embryonic brains on linear sucrose density gradients and examined the sedimentation pattern of Unkempt (Fig. 6A; Supplemental Fig. 8A). A significant proportion of Unkempt cosedimented with fractions containing heavy polyribosomes and showed a distribution akin to FMRP, a known polyribosome-associated protein (Stefani et al. 2004). Treatment of lysates with EDTA to dissociate the large from the small ribosomal subunits disrupted the polysomes and shifted Unkempt to lighter fractions. Binding of Unkempt to polyribosomes was also RNA-dependent, since digestion of the pooled heavy sucrose fractions with RNase I or micrococcal nuclease (MNase) quantitatively released Unkempt from ribosomes into the soluble fraction, similar to poly(A)-binding protein (PABP), while a component of the 40S ribosomal subunit (RPS3) was resistant to RNA cleavage (Fig. 6B). Taken together, these results suggest that the association of Unkempt with polyribosomes is dependent on Unkempt binding to both the ribosomes and the target mRNA.

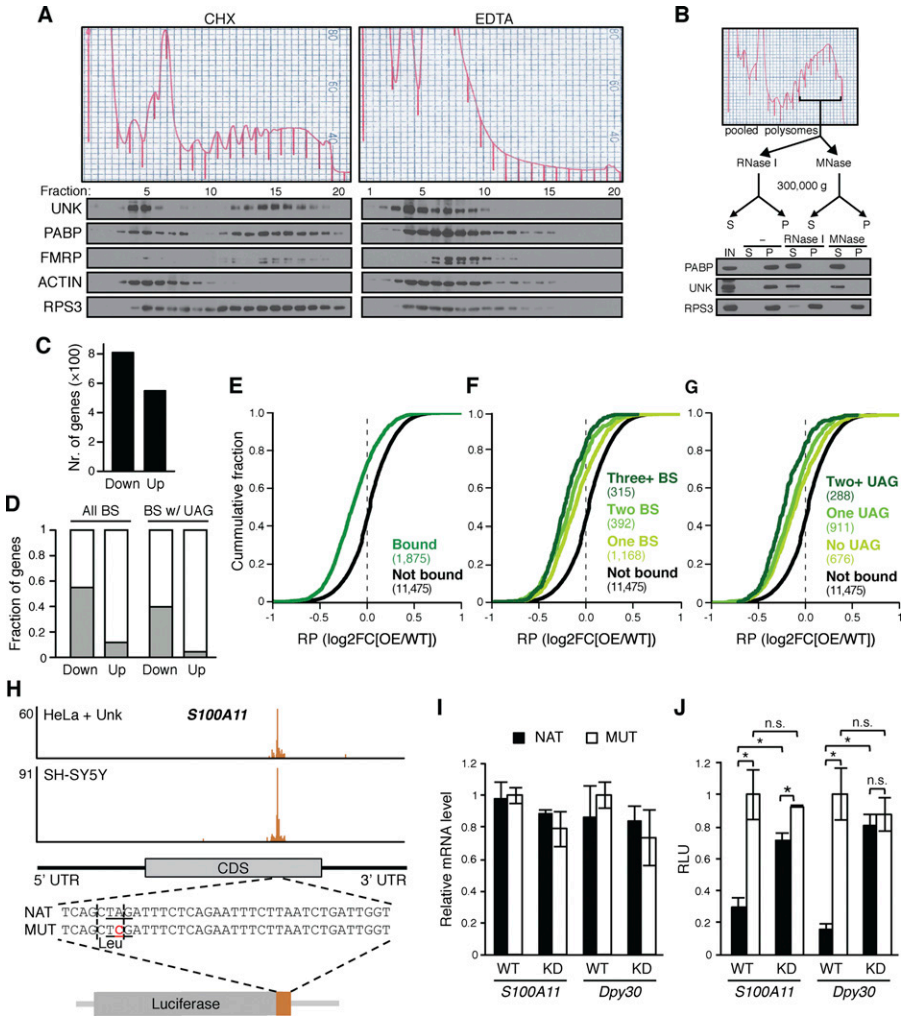

Figure 6. Unkempt represses translation of its target messages. (*A*,*B*) RNA-dependent association of Unkempt with polyribosomes. (*A*) Polysome profiling of SH-SY5Y cells harvested in the presence of cycloheximide (CHX) or EDTA and immunoblot analysis of individual fractions for the indicated proteins. See also Supplemental Figure S8A. (*B*) Digestion of polyribosomal fractions with RNase I or MNase followed by immunoblot analysis of the indicated proteins for their release into the supernatant (S) from the pelleted (P) fraction. (IN) Input. (*C*) Ribosome profiling data showing total numbers of genes with significantly decreased (Down) or increased (Up) RPF count in Dox-treated GFP and Unkempt-inducible versus GFP-only-inducible HeLa cells (false discovery rate [FDR] < 5%). (*D*) Fractions of genes with altered RPF counts as shown in *C* that are bound by Unkempt, considering all binding sites (All BS) or binding sites harboring the UAG motif (BS w/UAG). (*E–G*) Cumulative distributions of changes in ribosome occupancy for all transcripts containing Unkempt-binding sites (Bound); transcripts with one (One BS), two (Two BS), or three or more (Three+ BS) binding sites; transcripts without the UAG motif (No UAG), with one UAG motif (One UAG), or with two or more UAG motifs (Two+ UAG) within the binding sites; and control transcripts lacking Unkempt-binding sites (Not bound). The number of genes in each category is indicated in parentheses. Comparison of either set of Unkempt target transcripts with the nonbound controls showed a significant difference ($P < 0.0001$). (*H–J*) Translational repression by Unkempt requires the UAG motif. (*H*) Extension of the luciferase gene with native (NAT) or point-mutated (MUT) sequence corresponding to the Unkempt-binding site within the human *S100A11* transcript. The mutation in the critical UAG motif (underlined) preserves the amino acid (Leu) encoded by the affected codon (vertical dashed lines). (*I*,*J*) Dual-luciferase assay using the native or point-mutated hybrid luciferase in wild-type (WT) and Unkempt knockdown (KD) SH-SY5Y cells (see also Supplemental Fig. S9C). Relative levels of the hybrid luciferase transcripts (*I*) and relative luminescence units (RLU) (*J*) are shown. Error bars indicate SD ($n = 3$). (*) $P < 0.05$, Student's *t*-test.

In order to determine whether Unkempt directly impacts protein synthesis, we carried out ribosome profiling (Ingolia et al. 2009) to obtain a genome-wide view of ribosome occupancy on Unkempt target messages (Supplemental Fig. S8B). Comparative profiling of ribosome-protected fragments (RPFs) from HeLa cells with or without ectopic expression of Unkempt revealed several traits typical of translation, including 3-nucleotide (nt) periodicity, pausing of ribosomes in the proximity of start and stop codons, and retention of ribosomes in the 5′ untranslated region (UTR) segment (Supplemental Fig. S8C).

Changes in the rate of translation have been shown to correlate with changes in ribosome occupancy of mRNAs (Ingolia et al. 2009). Our global analysis of ribosome profiling data indicated a greater number of genes with a significantly reduced RPF count compared with genes with an increased RPF count upon induction of Unkempt in HeLa cells (Fig. 6C). Markedly, the bias became substantially more apparent when we considered the RNA-binding information; Unkempt was found to largely target genes with a reduced RPF count, and this trend was most prominent for the subset of target genes harboring the UAG motif within Unkempt-binding sites (Fig. 6D). These observations hinted at a repressive effect of Unkempt on translation of its bound transcripts.

To examine the global impact of Unkempt–RNA interactions on ribosome occupancy of the targeted transcripts, we binned the transcripts according to their binding to Unkempt, number of binding sites, and presence or absence of the UAG motif. Markedly, Unkempt target genes exhibited a significant drop in ribosome occupancy compared with nontargets, an effect that further increased in the presence of multiple binding sites (Fig. 6E–G). These data demonstrate that Unkempt reduces translational efficiency of its target mRNAs by lowering the ribosome occupancy without concurrent changes in transcript abundance. It should be noted that since only a fraction of all cells analyzed by ribosome profiling successfully induce Unkempt upon treatment with Dox (31%) (Supplemental Fig. S9A), the observed impact on translational efficiency is likely an underestimate of the repressive activity of Unkempt.

To validate the inhibitory effect of Unkempt on translation in neuronal cells, we carried out immunoblotting for high-confidence target genes that showed no significant changes at the transcript level upon knockdown in SH-SY5Y cells. Proteins CCT5, HNRNPK, and DDX5, all of which are encoded by mRNAs that rank among the top 10% of all Unkempt targets (Supplemental Table S2A), were expressed at notably higher levels in Unkempt-deficient compared with wild-type SH-SY5Y cells (Supplemental Fig. S9B). In contrast, nontarget controls—GAPDH and histone H3—were expressed at comparable levels in both conditions.

The RNA recognition element is required for translational control by Unkempt

To determine whether the translational repression of Unkempt target genes in vivo requires a direct interaction between Unkempt and the identified RNA recognition element, we used a modified dual-luciferase reporter assay. We took a well-defined RNA-binding site of a strong Unkempt target gene, *S100A11*, and inserted it proximal to the C terminus of the firefly luciferase gene so as to mimic the respective position in the endogenous gene while preserving the reading frame (Fig. 6H). We also prepared a mutant construct in which we converted the critical UAG motif into UCG, which retained the encoded amino acid (leucine) but abolished the binding by Unkempt, as informed by the EMSA assay (Fig. 5E). Upon transfection of either of these two constructs along with the Renilla luciferase vector into either control or Unkempt-depleted SH-SY5Y cells, we detected comparable levels of each modified luciferase mRNA by RT-qPCR analysis (Fig. 6I). However, measurements of luminescence in the control cells revealed about a threefold lower abundance of the modified luciferase produced from the construct containing the native binding site sequence (NAT) compared with the construct with the point mutation (MUT) (Fig. 6J). In contrast, Unkempt-depleted cells showed a much smaller, albeit significant, difference of ~25% in firefly luciferase activity. We repeated the experiment with a binding site of a different top-scoring mRNA target of Unkempt, *Dpy30*, and observed a similar if not more profound repressive effect of Unkempt–mRNA interaction on translation (about fivefold) that was essentially eliminated upon depletion of Unkempt (Fig. 6J; Supplemental Fig. S9C). Taken together, these data indicate that the translational control by Unkempt critically depends on recognition of its binding element within target mRNAs.

Similar to Unkempt, a few other RBPs have been proposed to largely act by regulating translation of target transcripts, although the mechanisms of their translational control are not well understood (Polesskaya et al. 2007; Abdelmohsen et al. 2011; Darnell et al. 2011; Peng et al. 2011; Cho et al. 2012; Kwan et al. 2012; Wilbert et al. 2012; Brummer et al. 2013). FMRP, which, like Unkempt, primarily targets coding regions of mRNAs, was shown to repress protein synthesis by stalling the translocating ribosomes (Darnell et al. 2011). However, a runoff experiment with puromycin revealed that Unkempt, unlike FMRP, shifted to lighter fractions of a sucrose gradient, suggesting its association with actively translocating but not stalled ribosomes (Supplemental Fig. S9D). Moreover, a global correlation of RNA-binding positions of Unkempt with ribosome profiling data unveiled enriched binding of Unkempt to sites on mRNAs just upstream of endogenously paused ribosomes, inconsistent with the ribosome stalling model in which an RBP would be expected to block the translocation of ribosomes and locate downstream from their clusters (Supplemental Fig. S9E). We hypothesize that translational repression by Unkempt entails a different process, such as interference with translation initiation, which is a generally rate-limiting and commonly regulated step (Supplemental Fig. S9F; Besse and Ephrussi 2008).

Discussion

Coregulation of physiologically related genes by RBPs has previously been linked with different aspects of cellular morphogenesis. For instance, in mammalian brains, a multitude of RBPs implicated in neurological disorders, including FUS, FMRP, NOVA, SAM68, and Staufen proteins, regulate mRNAs with synaptic functions and affect the morphology of neuronal dendritic spines (Fujii et al. 2005; Ule et al. 2005; Goetze et al. 2006; Dictenberg et al. 2008; Vessey et al. 2008; Ruggiu et al. 2009; Darnell et al. 2011; Iijima et al. 2011; Wagnon et al. 2012; Klein et al. 2013). In

contrast to these RBPs, our data suggest that Unkempt affects neuronal morphology by regulating a molecular program that is intrinsic to cells of diverse lineages. Such target selectivity may explain at least in part the capacity of ectopic Unkempt to establish a neuronal-like morphology in nonneuronal cells, further suggesting that tissues other than brain could use Unkempt for shaping of their cells. Consistent with this possibility, the initial report on Unkempt noted its widespread expression during the earliest stages of fruit fly development (Mohler et al. 1992), and expression analysis in mice indicates the presence of moderate levels of Unkempt in numerous tissues (Supplemental Fig. S1C). Future studies are warranted to investigate the effects of Unkempt on cell morphogenesis in different tissues. Of note, since acute gene silencing using shRNA delivery by in utero electroporation can lead to off-target effects and associated artifacts (Baek et al. 2014), in vivo analyses with additional, less error-prone approaches will be essential.

The mode of Unkempt binding to target mRNAs is unexpected and differs from that of most other RBPs studied to date. Indeed, the extent of sequence specificity of several other RBPs seems comparable with that of Unkempt, yet Unkempt exhibits a higher definition of binding. Thus, there likely exist additional determinants to guide Unkempt to its unique binding sites on cognate transcripts. This assumption is supported by the observation that the consensus Unkempt recognition element UAG_gap_WWW relatively poorly predicts the actual binding sites. By varying the length of the spacer (gap) between both motifs and the definition of the U/A-rich motif, we found that the sequences matching UAGNNUUU consensus predicted the actual binding sites with the greatest specificity; still, out of all sites within the CDS matching this sequence, only 23% were bound by Unkempt, representing just 11% of all Unkempt-binding sites in the CDS. We speculate that one auxiliary landmark could be provided by the proximity or cobinding of ribosomes, which could also reduce the need for sequence scanning by Unkempt along the targeted mRNA. However, the exact reason and the requirement, if any, for the commonly singular contact sites of Unkempt on mRNAs remain to be investigated.

The association of Unkempt with large polyribosomes along with its impact on ribosome occupancy of target mRNAs posit translation as a key post-transcriptional process regulated by Unkempt. The fact that Unkempt controls translation of proteins that themselves regulate translation as well as the cytoskeleton and trafficking suggests a highly hierarchical structure of the RNA operon in which Unkempt plays the role of the "regulator of the regulators." This idea is further supported by the finding of several RBPs (each regulating its own molecular program) among Unkempt targets, including PARK7, RBFOX2, Staufen proteins, ELAVL4, and several heterogeneous nuclear ribonucleoproteins (Supplemental Table S2). One implication of such hierarchical activity is that Unkempt does not need to act at the actual sites of structural rearrangements during morphogenesis but can instate through translational control a global molecular program that in turn remodels cellular morphology. It should be noted that Unkempt might regulate cell morphogenesis by additional means that are unrelated to its RNA binding in the cytoplasm, including, for example, a putative nuclear activity and interactions with other proteins.

Unkempt's sequence specificity, mode of mRNA binding, and potent impact on protein translation together form an RNA operon that can be extremely sensitive to mutations within the binding sites of Unkempt. As seen with point mutations of the hybrid luciferase transcripts, a single nucleotide exchange can have a profound effect on protein levels without affecting the transcript abundance or the encoded amino acid sequence. Broadly speaking, this suggests that synonymous genetic mutations, also known as "silent" mutations, could have a substantial impact on gene expression through the action of RBPs with narrowly defined position-dependent regulatory capacities comparable with that of Unkempt. With hundreds of unstudied RBPs encoded by the human genome, such sensitivity to point mutations could provide a novel explanation for the frequent but often neglected association of synonymous mutations with human disease. Given the severity of the phenotypes observed upon depletion of Unkempt in flies and mice, one could envision that such mutations or compromised activity of Unkempt protein itself would manifest in embryonic lethality or give rise to debilitating neurological disorders in humans.

Materials and methods

iCLIP experiments

All iCLIP experiments on SH-SY5Y cells, HeLa cells, and mouse embryonic brains were carried out in replicates using polyclonal rabbit anti-UNK antibody from Sigma (HPA023636) by adhering to a published protocol (Konig et al. 2011). See also the Supplemental Material.

RNA sequencing (RNA-seq)

RNA-seq libraries were prepared from total RNA extracted from SH-SY5Y cells transfected with nontargeting or UNK targeting siRNA as described in the Supplemental Material. Total RNA was polyA-selected, fragmented, reverse-transcribed, and sequenced according to the TruSeq protocol (Illumina).

Ribosome footprinting

HeLa cells inducibly expressing GFP and Unkempt or GFP alone were lysed, and the lysates were treated with RNase I and spun to pellet the ribosomes. Ribosome-protected RNA was isolated, and deep sequencing libraries were generated and sequenced as described in the Supplemental Material.

Polysome profiling

Whole mouse embryonic brains or SH-SY5Y cells were treated with cycloheximide, lysed, layered on top of a sucrose gradient, and centrifuged. The gradient was fractionated concomitant with recording of the absorbance, and proteins from each fraction were precipitated and analyzed by immunoblotting.

Purification of recombinant Unkempt and EMSAs

Full-length mouse Unkempt was purified from Dox-inducible HeLa S3 cells by immunoaffinity purification. Synthetic oligoribonucleotides were radioactively labeled and incubated with the recombinant Unkempt, and RNA binding was assessed by native gel electrophoresis.

Functional classification of Unkempt target genes

The enrichment of gene ontology categories in each set of Unkempt targets was analyzed using the online tool DAVID (http://david.abcc.ncifcrf.gov). Pathway analysis was performed using the Web-based Ingenuity Pathway Analysis program (Ingenuity Systems, http:// www.ingenuity.com).

Analysis of high-throughput sequencing data

Processing and genomic mapping of all high-throughput sequencing reads, including the analyses of differential transcript abundance (RNA-seq data), identification and characterization of Unkempt-binding sites (iCLIP data), and analyses of differential ribosome occupancy (ribosome profiling data), are described in detail in the Supplemental Material.

Accession numbers

The ArrayExpress accession numbers for the iCLIP, RNA-seq, and ribosome profiling data are E-MTAB-2279, E-MTAB-2277, and E-MTAB-2278, respectively.

Acknowledgments

We thank Yoichiro Sugimoto, Andrea D'Ambrogio, Tom Chittenden, and Angeles Fernandez-Gonzales for advice and assistance with the experiments; Timothy Mitchison, Julian König, Linda Van Aelst, Marc Kirschner, Nicholas Ingolia, David Pellman, David van Vactor, John Flanagan, and members of the Shi laboratory for discussion and comments on the manuscript; Črt Gorup for his work on the iCount pipeline; and Francois Guillemot for the pCAGGS-IRES-RFP vector. This study was supported by the Nancy Lurie Marks Post-doctoral Fellowship (J.M.), an EMBL Interdisciplinary Postdocs (EIPOD) fellowship (K.Z.), Stuart H.Q. and Victoria Quan Fellowship (Y.J.Y.), National Institute of General Medical Sciences grant T32GM007753 (Y.J.Y.), National Institute of Neurological Disorders and Stroke grants R01 NS032457 and R01 NS35129 (C.A.W.), the Manton Center for Orphan Disease Research (C.A.W.), and National Institutes of Health grants GM058012, CA118487, and MH096066 (Y.S.). C.A.W. is an Investigator of the Howard Hughes Medical Institute. Y.S. is an American Cancer Society Research Professor. Y.S. is also a cofounder of Constellation Pharmaceuticals, Inc., and a member of its scientific advisory board.

References

Abdelmohsen K, Tominaga K, Lee EK, Srikantan S, Kang MJ, Kim MM, Selimyan R, Martindale JL, Yang X, Carrier F, et al. 2011. Enhanced translation by Nucleolin via G-rich elements in coding and non-coding regions of target mRNAs. *Nucleic Acids Res* **39:** 8513–8530.

Avet-Rochex A, Carvajal N, Christoforou CP, Yeung K, Maierbrugger KT, Hobbs C, Lalli G, Cagin U, Plachot C, McNeill H, et al. 2014. Unkempt is negatively regulated by mTOR and uncouples neuronal differentiation from growth control. *PLoS Genet* **10:** e1004624.

Baek ST, Kerjan G, Bielas SL, Lee JE, Fenstermaker AG, Novarino G, Gleeson JG. 2014. Off-target effect of doublecortin family shRNA on neuronal migration associated with endogenous microRNA dysregulation. *Neuron* **82:** 1255–1262.

Besse F, Ephrussi A. 2008. Translational control of localized mRNAs: restricting protein synthesis in space and time. *Nat Rev Mol Cell Biol* **9:** 971–980.

Brummer A, Kishore S, Subasic D, Hengartner M, Zavolan M. 2013. Modeling the binding specificity of the RNA-binding protein GLD-1 suggests a function of coding region-located sites in translational repression. *RNA* **19:** 1317–1326.

Carballo E, Lai WS, Blackshear PJ. 1998. Feedback inhibition of macrophage tumor necrosis factor-α production by tristetraprolin. *Science* **281:** 1001–1005.

Cho J, Chang H, Kwon SC, Kim B, Kim Y, Choe J, Ha M, Kim YK, Kim VN. 2012. LIN28A is a suppressor of ER-associated translation in embryonic stem cells. *Cell* **151:** 765–777.

Darnell JC, Van Driesche SJ, Zhang C, Hung KY, Mele A, Fraser CE, Stone EF, Chen C, Fak JJ, Chi SW, et al. 2011. FMRP stalls ribosomal translocation on mRNAs linked to synaptic function and autism. *Cell* **146:** 247–261.

Davis RL, Weintraub H, Lassar AB. 1987. Expression of a single transfected cDNA converts fibroblasts to myoblasts. *Cell* **51:** 987–1000.

Dictenberg JB, Swanger SA, Antar LN, Singer RH, Bassell GJ. 2008. A direct role for FMRP in activity-dependent dendritic mRNA transport links filopodial-spine morphogenesis to fragile X syndrome. *Dev Cell* **14:** 926–939.

Dotti CG, Sullivan CA, Banker GA. 1988. The establishment of polarity by hippocampal neurons in culture. *J Neurosci* **8:** 1454–1468.

Fujii R, Okabe S, Urushido T, Inoue K, Yoshimura A, Tachibana T, Nishikawa T, Hicks GG, Takumi T. 2005. The RNA binding protein TLS is translocated to dendritic spines by mGluR5 activation and regulates spine morphology. *Curr Biol* **15:** 587–593.

Goetze B, Tuebing F, Xie Y, Dorostkar MM, Thomas S, Pehl U, Boehm S, Macchi P, Kiebler MA. 2006. The brain-specific double-stranded RNA-binding protein Staufen2 is required for dendritic spine morphogenesis. *J Cell Biol* **172:** 221–231.

Hall TM. 2005. Multiple modes of RNA recognition by zinc finger proteins. *Curr Opin Struct Biol* **15:** 367–373.

Iijima T, Wu K, Witte H, Hanno-Iijima Y, Glatter T, Richard S, Scheiffele P. 2011. SAM68 regulates neuronal activity-dependent alternative splicing of Neurexin-1. *Cell* **147:** 1601–1614.

Ince-Dunn G, Okano HJ, Jensen KB, Park WY, Zhong R, Ule J, Mele A, Fak JJ, Yang C, Zhang C, et al. 2012. Neuronal Elav-like (Hu) proteins regulate RNA splicing and abundance to control glutamate levels and neuronal excitability. *Neuron* **75:** 1067–1080.

Ingolia NT, Ghaemmaghami S, Newman JR, Weissman JS. 2009. Genome-wide analysis in vivo of translation with nucleotide resolution using ribosome profiling. *Science* **324:** 218–223.

Keene JD. 2007. RNA regulons: coordination of post-transcriptional events. *Nat Rev Genet* **8:** 533–543.

Kent WJ, Sugnet CW, Furey TS, Roskin KM, Pringle TH, Zahler AM, Haussler D. 2002. The human genome browser at UCSC. *Genome Res* **12:** 996–1006.

Klein ME, Younts TJ, Castillo PE, Jordan BA. 2013. RNA-binding protein Sam68 controls synapse number and local β-actin mRNA metabolism in dendrites. *Proc Natl Acad Sci* **110:** 3125–3130.

Konig J, Zarnack K, Rot G, Curk T, Kayikci M, Zupan B, Turner DJ, Luscombe NM, Ule J. 2010. iCLIP reveals the function of hnRNP particles in splicing at individual nucleotide resolution. *Nat Struct Mol Biol* **17:** 909–915.

Konig J, Zarnack K, Rot G, Curk T, Kayikci M, Zupan B, Turner DJ, Luscombe NM, Ule J. 2011. iCLIP—transcriptome-wide mapping of protein–RNA interactions with individual nucleotide resolution. *J Vis Exp*. **50:** e2638.

Kwan KY, Lam MM, Johnson MB, Dube U, Shim S, Rasin MR, Sousa AM, Fertuzinhos S, Chen JG, Arellano JI, et al. 2012. Species-dependent posttranscriptional regulation of NOS1 by FMRP in the developing cerebral cortex. *Cell* **149:** 899–911.

Leppek K, Schott J, Reitter S, Poetz F, Hammond MC, Stoecklin G. 2013. Roquin promotes constitutive mRNA decay via a conserved class of stem-loop recognition motifs. *Cell* **153:** 869–881.

Li X, Quon G, Lipshitz HD, Morris Q. 2010. Predicting in vivo binding sites of RNA-binding proteins using mRNA secondary structure. *RNA* **16:** 1096–1107.

Liang J, Song W, Tromp G, Kolattukudy PE, Fu M. 2008. Genome-wide survey and expression profiling of CCCH-zinc finger family reveals a functional module in macrophage activation. *PLoS ONE* **3:** e2880.

Lunde BM, Moore C, Varani G. 2007. RNA-binding proteins: modular design for efficient function. *Nat Rev Mol Cell Biol* **8:** 479–490.

Matsushita K, Takeuchi O, Standley DM, Kumagai Y, Kawagoe T, Miyake T, Satoh T, Kato H, Tsujimura T, Nakamura H, et al. 2009. Zc3h12a is an RNase essential for controlling immune responses by regulating mRNA decay. *Nature* **458:** 1185–1190.

Miller JW, Urbinati CR, Teng-Umnuay P, Stenberg MG, Byrne BJ, Thornton CA, Swanson MS. 2000. Recruitment of human muscleblind proteins to (CUG)(n) expansions associated with myotonic dystrophy. *EMBO J* **19:** 4439–4448.

Mohler J, Weiss N, Murli S, Mohammadi S, Vani K, Vasilakis G, Song CH, Epstein A, Kuang T, English J, et al. 1992. The embryonically active gene, *unkempt*, of *Drosophila* encodes a Cys3His finger protein. *Genetics* **131:** 377–388.

Niehrs C, Pollet N. 1999. Synexpression groups in eukaryotes. *Nature* **402:** 483–487.

Noctor SC, Martinez-Cerdeno V, Ivic L, Kriegstein AR. 2004. Cortical neurons arise in symmetric and asymmetric division zones and migrate through specific phases. *Nat Neurosci* **7:** 136–144.

Peng S, Chen LL, Lei XX, Yang L, Lin H, Carmichael GG, Huang Y. 2011. Genome-wide studies reveal that Lin28 enhances the translation of genes important for growth and survival of human embryonic stem cells. *Stem Cells* **29:** 496–504.

Polesskaya A, Cuvellier S, Naguibneva I, Duquet A, Moss EG, Harel-Bellan A. 2007. Lin-28 binds IGF-2 mRNA and participates in skeletal myogenesis by increasing translation efficiency. *Genes Dev* **21:** 1125–1138.

Ray D, Kazan H, Cook KB, Weirauch MT, Najafabadi HS, Li X, Gueroussov S, Albu M, Zheng H, Yang A, et al. 2013. A compendium of RNA-binding motifs for decoding gene regulation. *Nature* **499:** 172–177.

Rounbehler RJ, Fallahi M, Yang C, Steeves MA, Li W, Doherty JR, Schaub FX, Sanduja S, Dixon DA, Blackshear PJ, et al. 2012. Tristetraprolin impairs myc-induced lymphoma and abolishes the malignant state. *Cell* **150:** 563–574.

Ruggiu M, Herbst R, Kim N, Jevsek M, Fak JJ, Mann MA, Fischbach G, Burden SJ, Darnell RB. 2009. Rescuing Z+ agrin splicing in Nova null mice restores synapse formation and unmasks a physiologic defect in motor neuron firing. *Proc Natl Acad Sci* **106:** 3513–3518.

Sato T, Katagiri K, Gohbara A, Inoue K, Ogonuki N, Ogura A, Kubota Y, Ogawa T. 2011. In vitro production of functional sperm in cultured neonatal mouse testes. *Nature* **471:** 504–507.

Srivastava M, Simakov O, Chapman J, Fahey B, Gauthier ME, Mitros T, Richards GS, Conaco C, Dacre M, Hellsten U, et al. 2010. The *Amphimedon queenslandica* genome and the evolution of animal complexity. *Nature* **466:** 720–726.

Stefani G, Fraser CE, Darnell JC, Darnell RB. 2004. Fragile X mental retardation protein is associated with translating polyribosomes in neuronal cells. *J Neurosci* **24:** 7272–7276.

Sugimoto Y, Konig J, Hussain S, Zupan B, Curk T, Frye M, Ule J. 2012. Analysis of CLIP and iCLIP methods for nucleotide-resolution studies of protein–RNA interactions. *Genome Biol* **13:** R67.

Uehata T, Iwasaki H, Vandenbon A, Matsushita K, Hernandez-Cuellar E, Kuniyoshi K, Satoh T, Mino T, Suzuki Y, Standley DM, et al. 2013. Malt1-induced cleavage of regnase-1 in $CD4^+$ helper T cells regulates immune activation. *Cell* **153:** 1036–1049.

Ule J, Ule A, Spencer J, Williams A, Hu JS, Cline M, Wang H, Clark T, Fraser C, Ruggiu M, et al. 2005. Nova regulates brain-specific splicing to shape the synapse. *Nat Genet* **37:** 844–852.

Vessey JP, Macchi P, Stein JM, Mikl M, Hawker KN, Vogelsang P, Wieczorek K, Vendra G, Riefler J, Tubing F, et al. 2008. A loss of function allele for murine Staufen1 leads to impairment of dendritic Staufen1-RNP delivery and dendritic spine morphogenesis. *Proc Natl Acad Sci* **105:** 16374–16379.

Vierbuchen T, Ostermeier A, Pang ZP, Kokubu Y, Sudhof TC, Wernig M. 2010. Direct conversion of fibroblasts to functional neurons by defined factors. *Nature* **463:** 1035–1041.

Vinuesa CG, Cook MC, Angelucci C, Athanasopoulos V, Rui L, Hill KM, Yu D, Domaschenz H, Whittle B, Lambe T, et al. 2005. A RING-type ubiquitin ligase family member required to repress follicular helper T cells and autoimmunity. *Nature* **435:** 452–458.

Wagnon JL, Briese M, Sun W, Mahaffey CL, Curk T, Rot G, Ule J, Frankel WN. 2012. CELF4 regulates translation and local abundance of a vast set of mRNAs, including genes associated with regulation of synaptic function. *PLoS Genet* **8:** e1003067.

Wang ET, Cody NA, Jog S, Biancolella M, Wang TT, Treacy DJ, Luo S, Schroth GP, Housman DE, Reddy S, et al. 2012. Transcriptome-wide regulation of pre-mRNA splicing and mRNA localization by muscleblind proteins. *Cell* **150:** 710–724.

Wilbert ML, Huelga SC, Kapeli K, Stark TJ, Liang TY, Chen SX, Yan BY, Nathanson JL, Hutt KR, Lovci MT, et al. 2012. LIN28 binds messenger RNAs at GGAGA motifs and regulates splicing factor abundance. *Mol Cell* **48:** 195–206.